3D large deformation modeling of the 2020 Gjerdrum quick clay landslide

Quoc-Anh Tran[1], Agnete Rogstad[1], Ivan Depina[1], Fabricio Fernández[2], Gebray Habtu Alene[1], Gustav Grimstad[1], Steinar Nordal[1]

[1] Department of Civil and Environmental Engineering, Norwegian University of Science and Technology, Norway.

[2] Departamento de Ingeniería Civil, Universidad Católica del Norte, Antofagasta, Chile.

ABSTRACT

A quick clay slide in Gjerdrum, Norway, occurred at 4 a.m. on 30th December 2020 killing 10 people and destroying houses, roads, and other infrastructures. Approximately 1.35 million cubic meters of clay were released, a large volume liquefied, and debris was transported almost two kilometers downstream. An investigation following the slide determined that the slide was initialized in a 30-meter-high slope after 2-to-2,5-meter vertical erosion in a small creek running along the toe of the slope. After the initiation, the slide developed retrogressively in the order of 500 meters backward and sideways over a period of about 2 minutes. A conventional geotechnical slope stability analysis explains the initial slide. However, more advanced numerical tools are needed to simulate the retrogressive mechanism and the debris flow. The aim of the paper is to demonstrate a 3D Material Point Method model to capture some of the mechanisms involved from initiation until the debris comes to rest, and how this method can be used to reproduce and study the processes involved in large deformation landslides.

KEYWORKS: quick clay, sensitive clay landslides, Material Point Method, large deformation modeling

1 Introduction

Scandinavia and Canada are at risk of large-scale, sensitive clay landslides. For example, Norway has experienced large, quick clay landslides larger than 50.000m^3 approximately once per year since 1970 (J.S. L'Heureux, 2018). A tragic example occurred in December 2020 when a fatal sensitive clay landslide in Gjerdrum, Norway claimed ten lives and caused extensive damage to homes and infrastructure (Figure 1). These landslides are predominantly progressive or retrogressive due to significant softening behaviour of the sensitive clays after reaching peak strength. The Gjerdrum landslide was classified as a quick clay retrogressive flow landslide under the Varnes' classification of landslides (Hungr et al., 2014). This failure mechanism is typical in Norway. A retrogressive quick clay landslide has three phases: an initial slide in the triggering phase, the growth of the unstable soil volume and the post-failure mass flow phase. In the triggering phase, natural factors such as erosion or human activity initiates a small slide. Following this initiation, the involved soil mass liquefies and flows out of the slide pit, leaving behind a steep and often unstable back scarp. In the case of the Gjerdrum landslide, erosion is believed to have been the triggering event and the primary cause of the disaster (Ryan et al., 2021). Detailed studies of Lidar data revealed that the creek at the bottom of the slope had eroded 2-2.5 m vertically from 2007 to 2020 (Figure 2). The Gjerdrum landslide is reported to have occurred retrogressively in nine stages (Figure 3). This conclusion was drawn from various sources, including photos, videos, geotechnical and hydrogeological investigations, and witness testimony.

Figure 1 Gjerdrum landslide (photo from NVE)

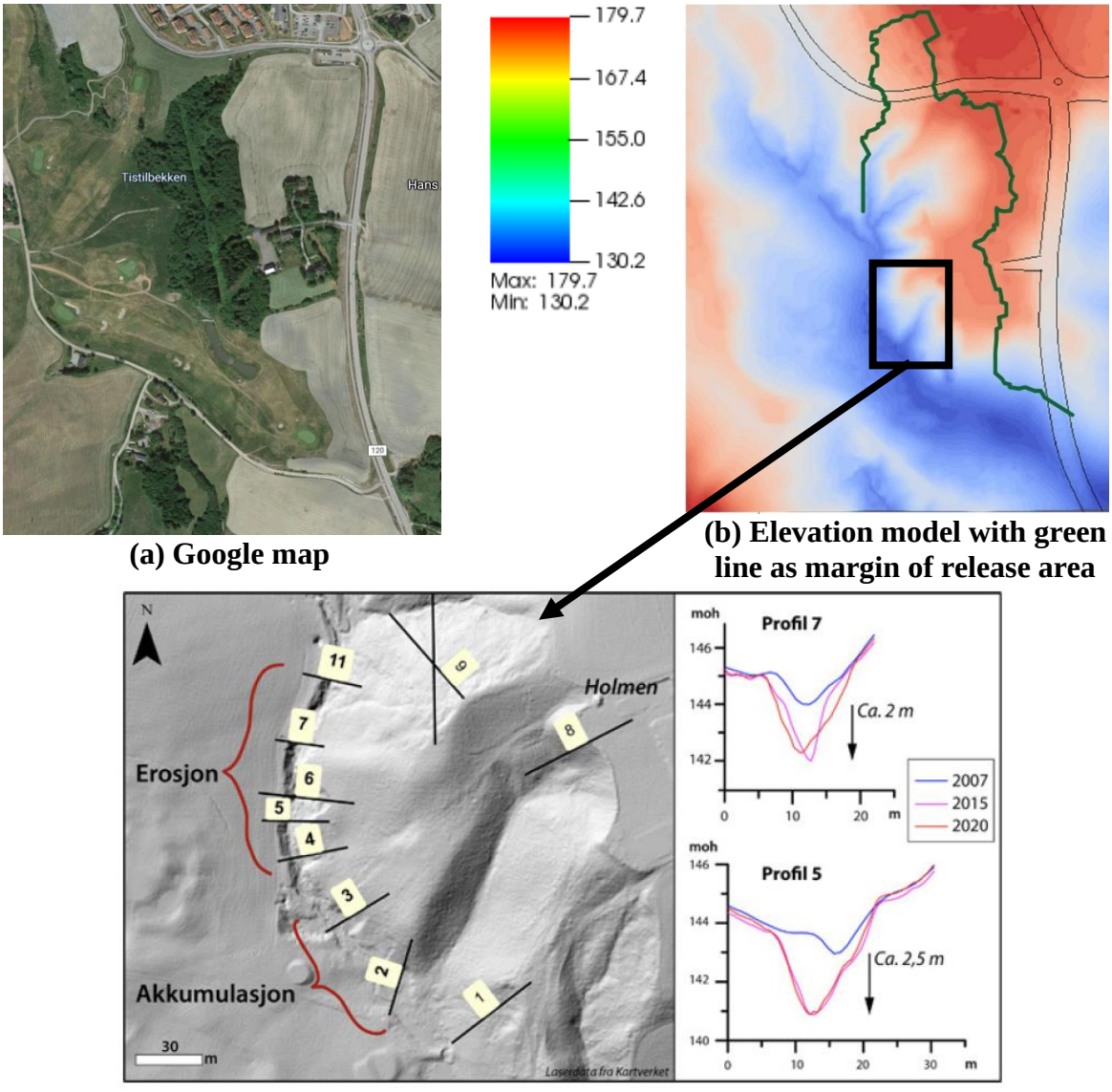

(a) Google map

(b) Elevation model with green line as margin of release area

(c) Erosion monitoring

Figure 2 Erosion mechanism (Ryan et al., 2021)

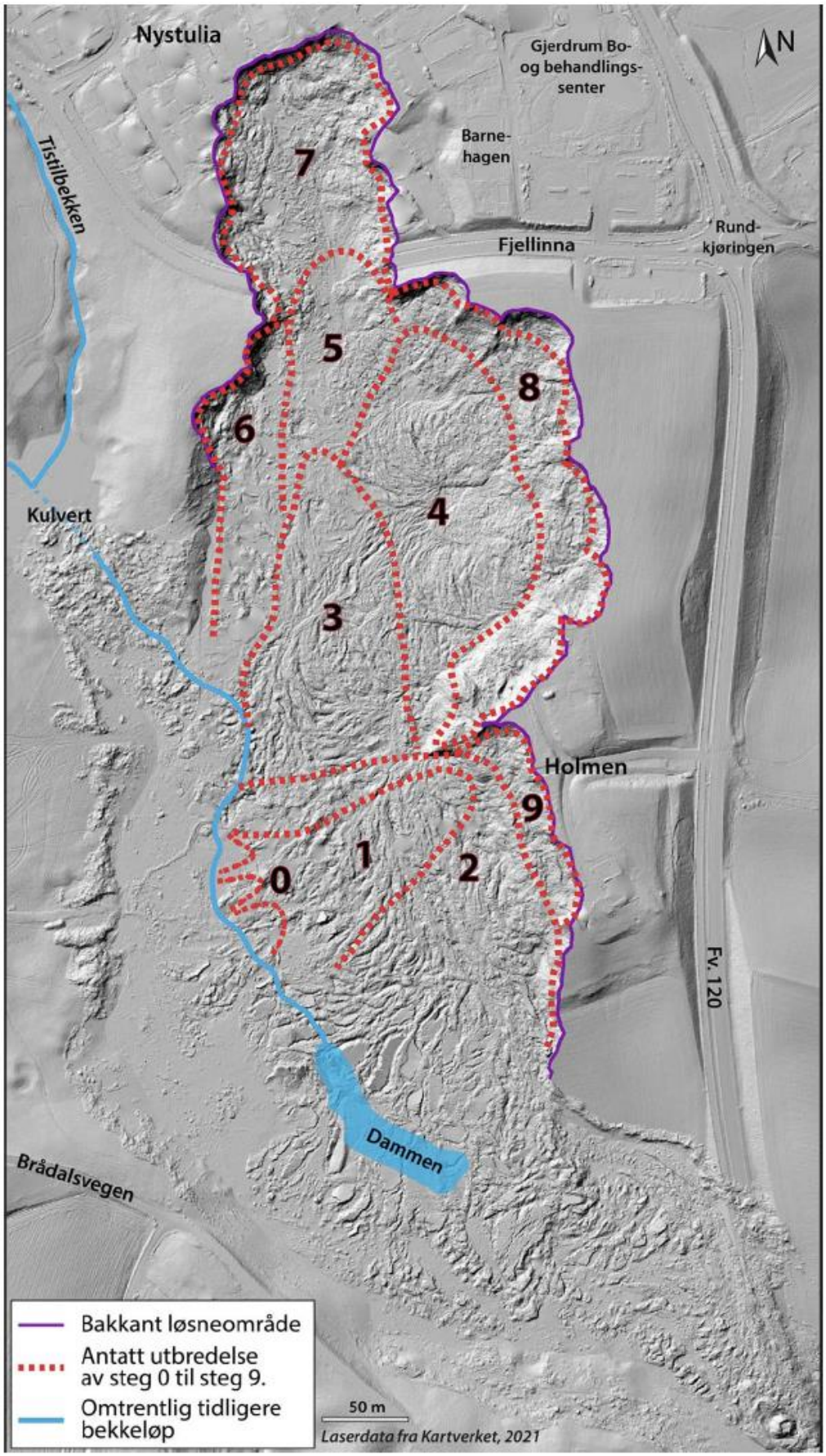

Figure 3 The nine stage of the Gjerdrum landslide (Ryan et al., 2021)

It is essential to model the initiation and mobility of quick clay landslides to improve future quick clay landslide risk management. Although conventional Finite Element or Limit Equilibrium methods can be used to determine the margin against failure (Grimstad et al., 2022; Locat et al., 2013; Locat et al., 2011), they are insufficient for capturing the mobility and development of the landslide. The mass movement can be modeled by incorporating depth-averaged balance equations, enabling us to analyze the motion of the soil masses in quick clay landslides (Liu et al., 2021). However, these depth-averaged models are incapable of replicating the nature of retrogression. Furthermore, the depth average models require to determine how much soil is released in advance. However, this should be determined implicitly as a result from the simulation.

Hence, particle-based methods have gained popularity as numerical tools for analyzing both the initiation and mobility of sensitive clay landslides. Examples include the coupled Lagrangian-Eulerian method (Dey et al., 2015), the Material Point Method (Tran & Solowski, 2019) , and the Particle Finite Element Method (Zhang et al., 2020). Notably, these studies have been conducted under plane strain conditions without accounting for three-dimensional effects. Nevertheless, when dealing with natural slopes characterized by layered soils and complex topography, slope stability analyses for two-dimensional and three-dimensional slopes can yield significantly different results (Alison McQuillan, 2021).

This study uses the Material Point Method to perform a 3D analysis of the Gjerdrum quick clay landslide as a case study. To understand the advantages and limitations of the model, the simulation results are compared to field observations from Gjerdrum. The 3D Material Point Method allows for the simulation of (1) the failure initiation associated with strain localization and (2) the mobility of the liquefied soil such as the size, direction, and distance of progressive failure.

2 Research Methodology

The 3D simulation of the Gjerdrum quick clay landslide presented in this paper is based on three key components as shown in Figure 4:

- A digital 3D model defining the terrain, depth to bedrock and soil layering

- A constitutive model with soil parameters for all soil layers.

- A numerical large deformation model using the Material Point Method.

The simulation involves model initialization, the triggering process, the liquefaction and some simplifying assumptions. The following sections present more details of the key components and the assumptions made.

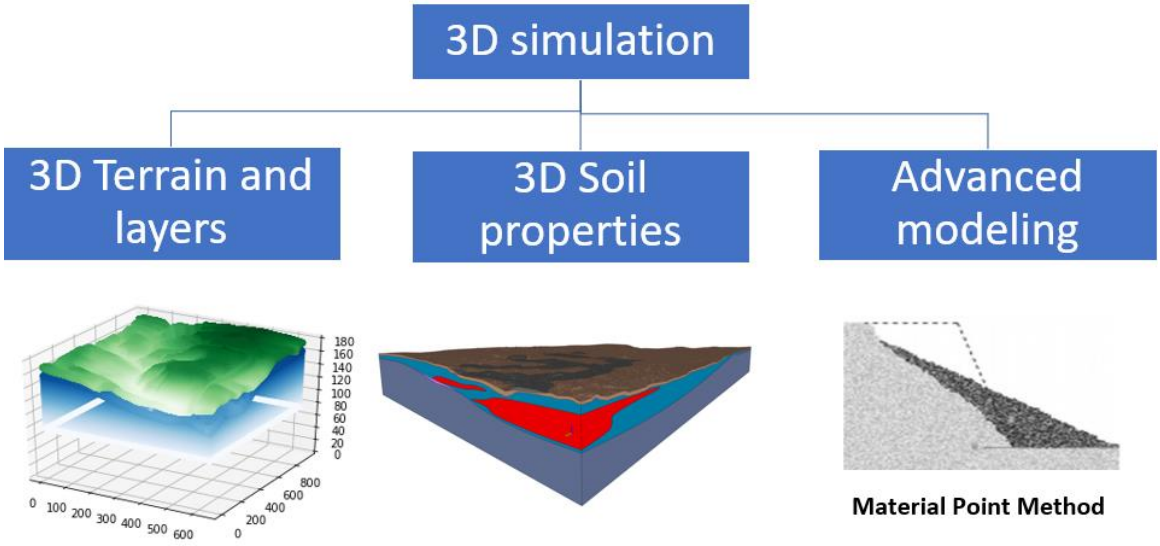

Figure 4 Framework for three-dimensional modelling of the Gjerdrum quick clay landslide

2.1 Undrained Elastoplastic Tresca Model

Given the rapid nature of the landslide, undrained conditions are assumed. An elastoplastic Tresca model is used to represent the undrained behavior of the clay. The model incorporates shear strength degradation as shown in Figure 5, where the strength decreases with increasing plastic shear strains. The degradation is described by:

$$s_u(\gamma, S_t) = s_{u,ref}[\frac{1}{S_t} + (1 - \frac{1}{S_t})e^{-3\gamma/\gamma_{95}}] \quad (1)$$

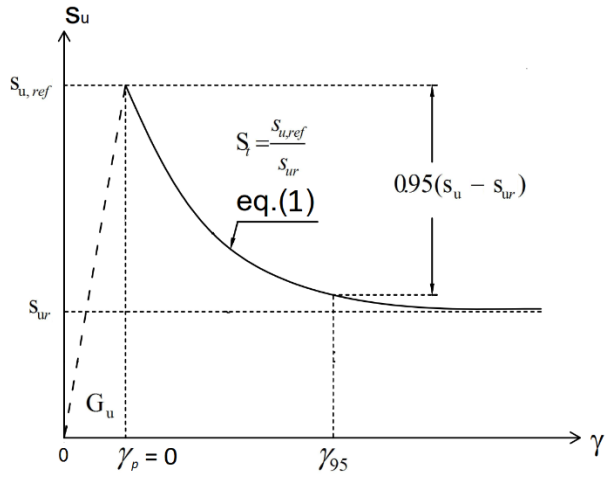

Figure 5 Constitutive model for sensitive clays

where γ is the current accumulated shear strain, γ_{95} is the accumulated shear strains required to obtain 95% reduction of shear strength and the sensitivity S_t is the ratio of undisturbed over remoulded undrained shear strength s_{ur}:

$$S_t = \frac{s_{u,ref}}{s_{ur}} \quad (2)$$

2.2 Soil Layer Classifications

Soil layers, as per soil investigations, consist of three main layers: bedrock, non-sensitive clay, and quick clay. Bedrock is considered rigid, non-sensitive clay layers are modeled with a Tresca softening model and low sensitivity (1-10), while quick clay layers are modeled using the Tresca softening model with high sensitivity (20-100). The undrained shear strengths are obtained from CPTUs retrieved from soil investigation reports (Multiconsult, 2021a-b) for the entire area.

2.3 Two Phases of Simulation

The simulation is divided into two phases:

- Phase 1: Establishing initial stresses under gravity using the estimated topography data from 2007.

- Phase 2: Utilizing the undrained soil properties to study the retrogressive failure process. For initiation of the slide, the topographical differences between 2015 and 2007 are removed to mimic erosion. Given negligible erosion between 2015 and 2020 (see Figure 2), the topography of 2015 represents the initial terrain elevation before the slide. Terrain elevation and soil layer data are sourced from the 3D LeapFrog model (Multiconsult, 2021a-b).

2.4 Model Scope and Limitations

The model focuses on the analysis of the triggering and retrogressive failure mechanism. The model does not account for several important factors related to the failure including soil anisotropy, hydraulic conditions, weather conditions, external loads attributable to buildings, or snow accumulations.

In the upcoming sections, we will delve into each of these components in detail, including the 3D reconstruction of terrain and soil layers, the assignment of soil properties to material points, and the application of the Material Point Method for modeling large deformations.

3 Three-dimensional terrain and layer model reconstruction

Spatial discretization of material points to represent the terrain and various soil layers is required to perform three-dimensional landslide modeling. We utilized LeapFrog data (Multiconsult, 2021a-b) containing detailed digital elevation information for the terrains and all soil layers, as depicted in Figure 6 and Figure 7 respectively. These data include the coordinates of layer interfaces labeled as $z_0 – z_5$ as depicted in Figure 8. To convert this data into numerical spatial discretization, we applied the 3D Material Point Method (MPM) discretization technique (Fernandez et al., 2020).

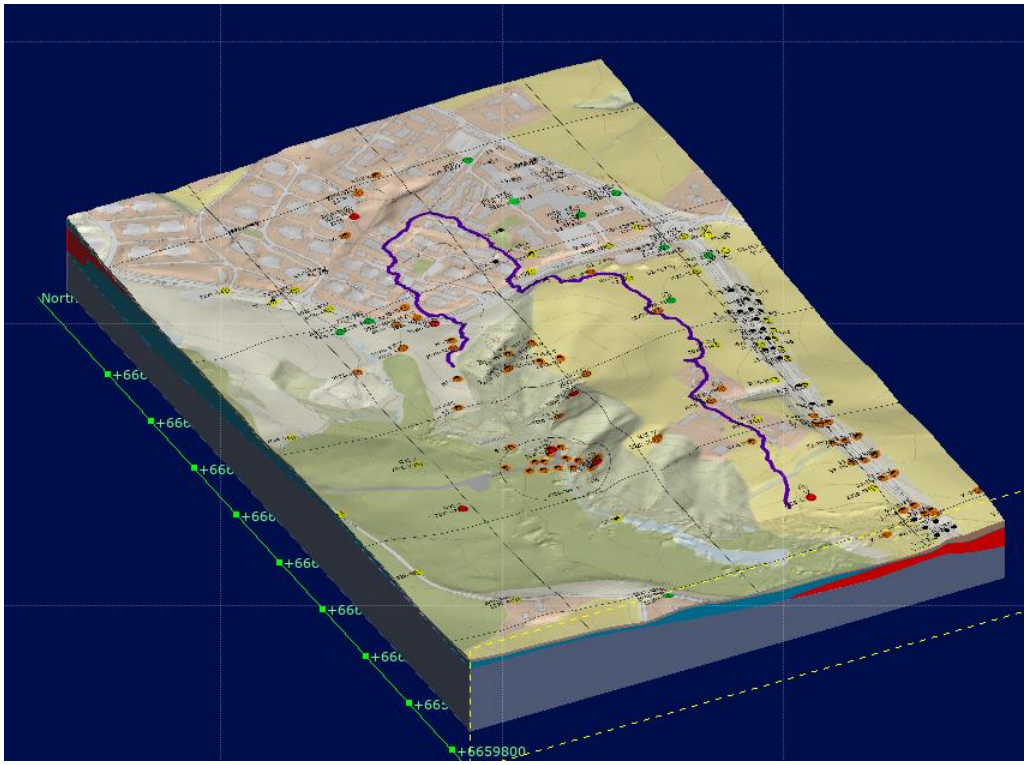

Figure 6 Terrain model in LeapFrog (Multiconsult, 2021a-b)

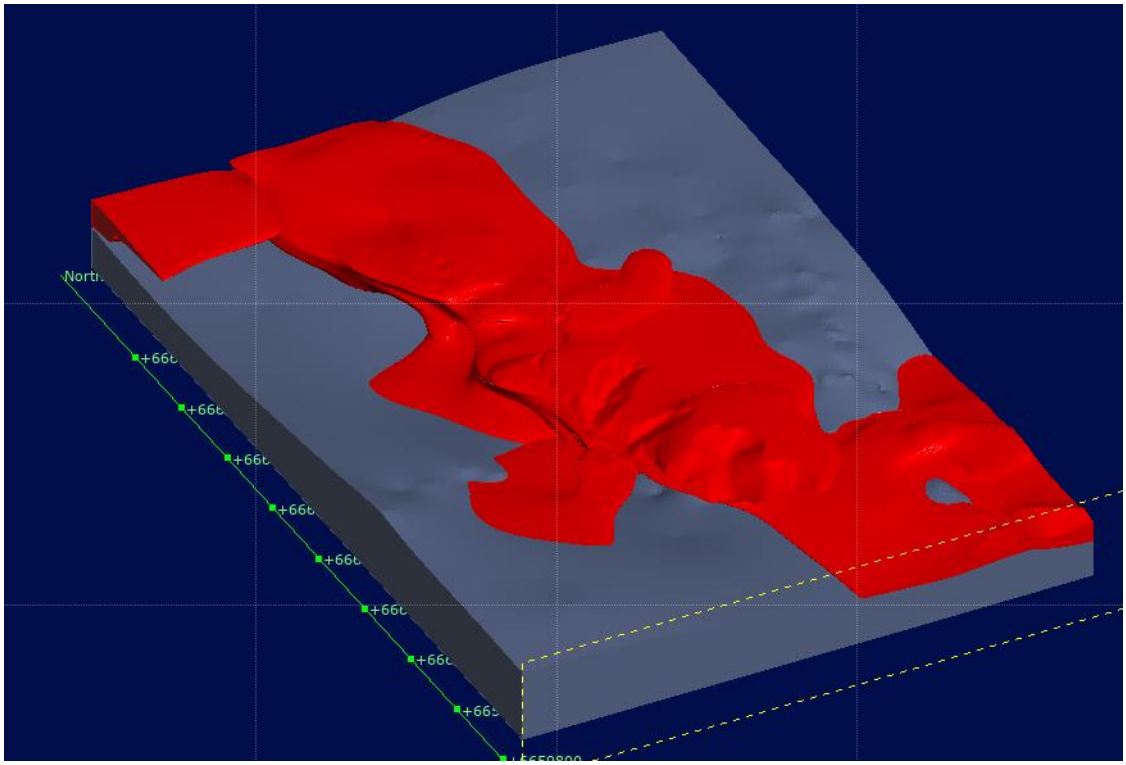

Figure 7 Bedrock (gray) and quick clay (red) layer in LeapFrog (Multiconsult, 2021a-b)

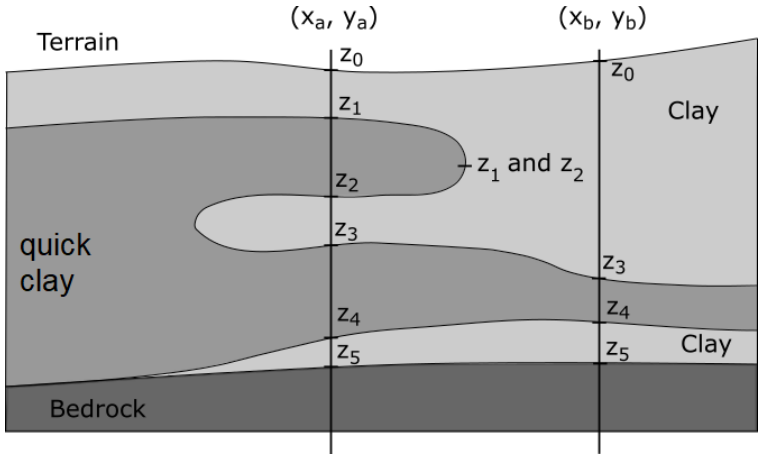

Figure 8 Input data for reconstruction of soil layers in LeapFrog

In this technique, we generated material points from the bottom of the bedrock up to the terrain level. Subsequently, based on the vertical coordinates of these material points, we assigned them to specific soil layers. For instance, material points falling between z_3 and z_4 were designated to the quick clay layers. This approach facilitated the creation of a 3D MPM model capable of accommodating arbitrary and complex distributions of soil layers and terrain within the analysis domain.

In summary, we transformed the LeapFrog data into different soil layers using 3D spatial discretization of material points. Figure 9, Figure 10 Figure 11 show the top elevation of the terrain, bedrock and quick clay layers respectively. The 3D model in this study featured a grid resolution of 1 meter cube with 8 material points per element, resulting in a distribution of 117,552,926 material points across a structured grid comprising 45,924,000 elements. Specifically, there were 89,471,948 material points in the non-sensitive clay and 28,080,978 material points in the quick clay layer.

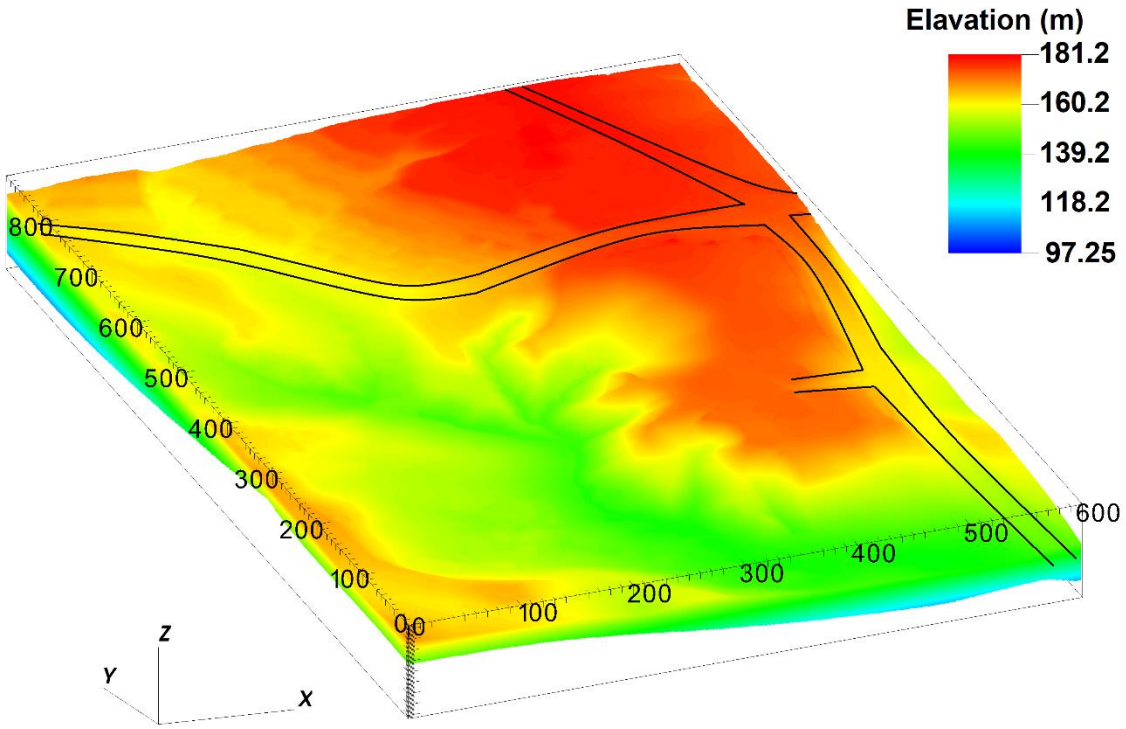

147

148 **Figure 9 Terrain elevation in numerical model in meters above sea level.**

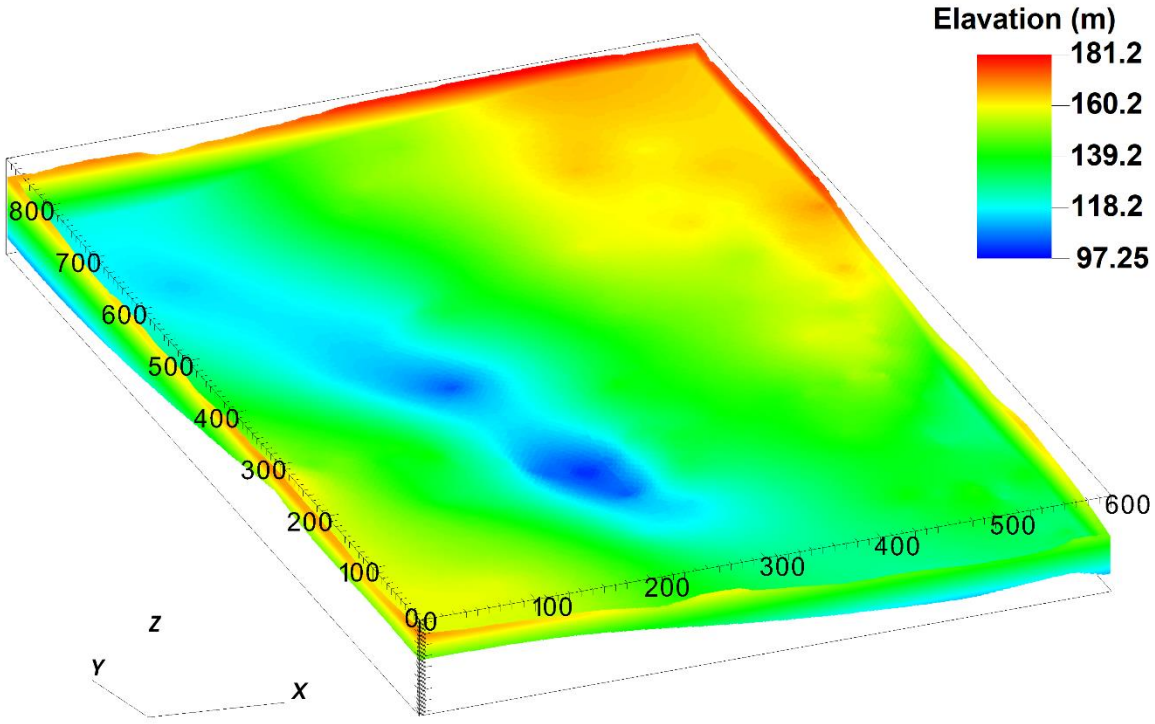

149

150 **Figure 10 Bedrock elevation in numerical model in meters above sea level.**

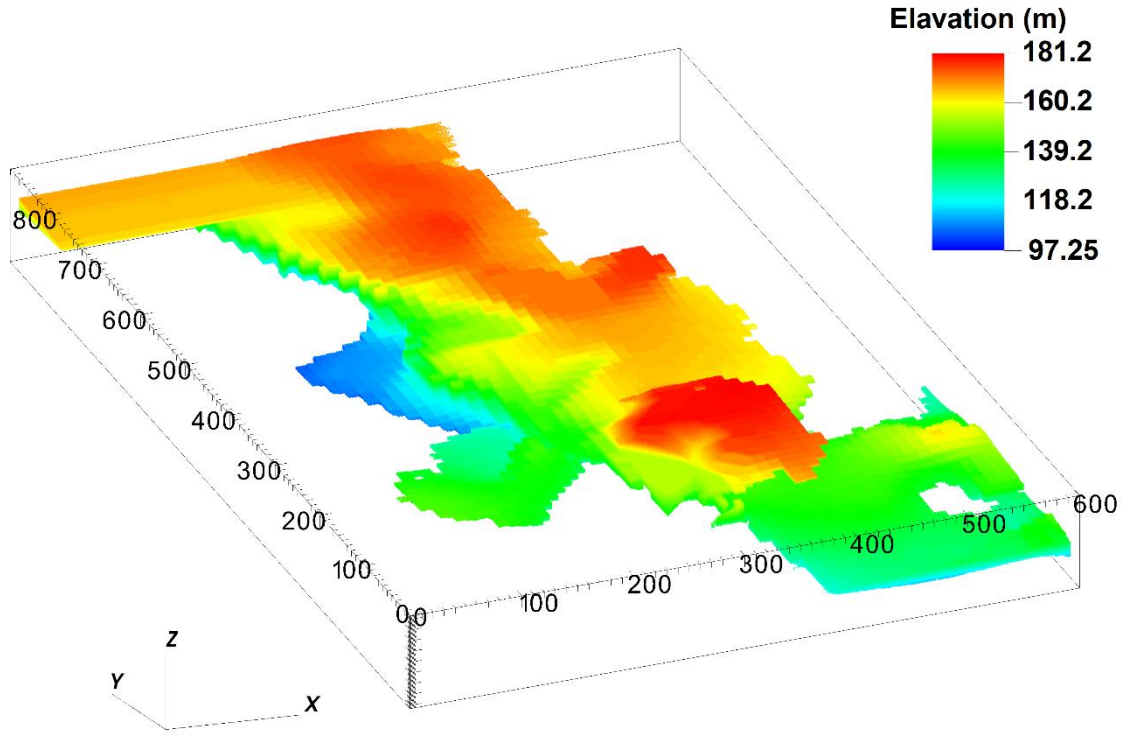

Figure 11 Top elevation of quick clay layer in numerical model in meters above sea level.

4 Assigning 3D soil properties for material points from CPTUs

After modelling soil layers, it is necessary to assign soil properties, including the undrained shear strength, to all material points. We employed data from 33 CPTu boreholes at the site (Figure 12). The undrained shear strength values in the boreholes are interpreted from available CPTu profiles and laboratory tests (Multiconsult, 2021a-a) and reduced to linear profiles along the depth for improved interpretability. Prior to implementing interpolation, each borehole was discretized into 200 observation points, denoted as $\mathbf{u}_i$ along the vertical axis. The values of the undrained shear strength, denoted as $s_u(\mathbf{u}_i)$, were interpolated at these points along the boreholes.

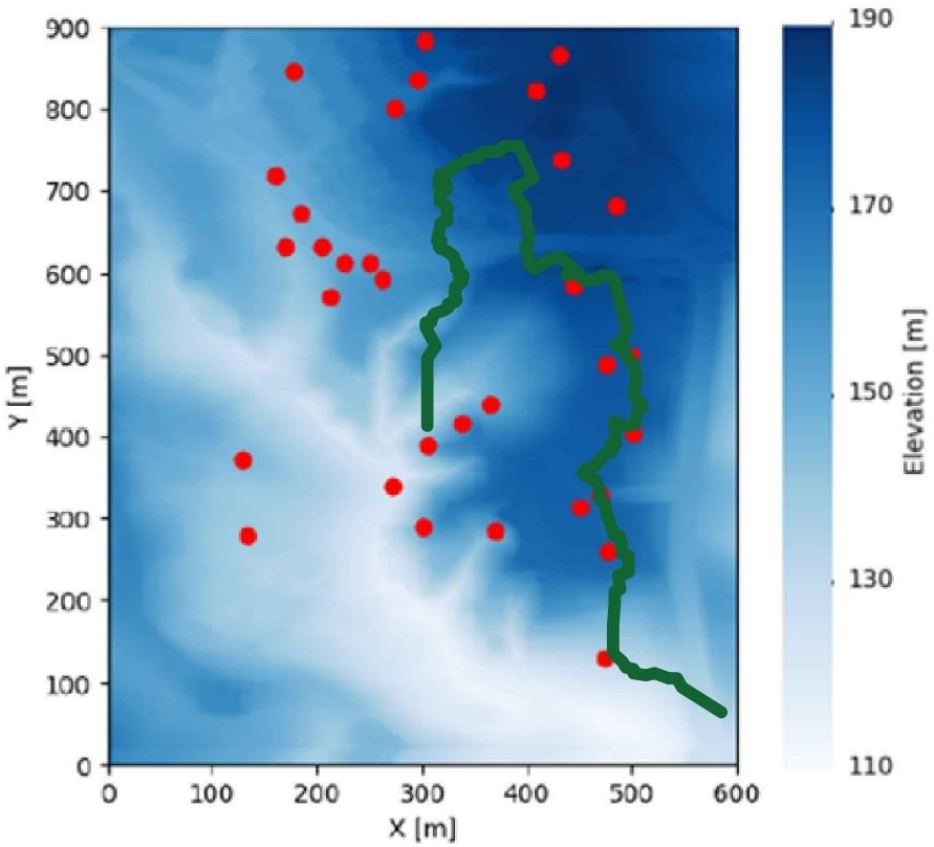

163

164 **Figure 12 Location of CPTU boreholes, with green line as margin of release area**

165 To interpolate the undrained shear strength values to any arbitrary material points located at
166 $\mathbf{u} = [x, y, z]^T$, we established a function of the undrained shear strength $s_u(\mathbf{u})$ in three
167 dimensions using a Radial Basis Function approximation (Rippa, 1999; Virtanen et al., 2020).
168 This function can be expressed as:

$$s_u(\mathbf{u}) = \sum_{i=1}^{n} a_i \, \varphi(\|\mathbf{u} - \mathbf{u}_i\|) \tag{3}$$

169 where φ is a fixed real-valued radial basis function and $\|\cdot\|$ denotes the Euclidean norm. The
170 points $\mathbf{u}_i; i = 1, \ldots, n$ correspond to the locations of points in the CPTU boreholes where the
171 value of undrained shear strength, $s_u(\mathbf{u}_i)$, is known.

172 In this function, it is necessary to select the radial basis function φ and compute the coefficients
173 a_i. Commonly used radial basis functions include Gaussian, cubic, linear, inverse, and
174 multiquadric. In this case, the linear radial basis function was chosen for the interpolation of

undrained shear strength values. The radial basis function's domain is assumed to have a radius of 10 meters. This selection offers computational efficiency and provides a more realistic representation, as the undrained shear strength typically increases linearly with depth. Additionally, the linear basis function does not require tuning parameters (Virtanen et al., 2020). The Radial Basis Function interpolation of the undrained shear strength values was implemented using the Python SciPy library (Virtanen et al., 2020).

Once the radial basis function is selected, the next step is to compute the coefficients, a_i, by solving the linear system represented as:

$$\mathbf{Aa} = \mathbf{f} \tag{4}$$

where $\mathbf{A} = A_{ij} = \varphi\left(\left\|\mathbf{u}_i - \mathbf{u}_j\right\|\right)$; $\mathbf{a} = [a_1, \dots, a_n]^T$; and $\mathbf{f} = [s_u(\mathbf{u_1}), \dots, s_u(\mathbf{u}_n)]^T$

After computing the coefficients, we can determine the undrained shear strength for all the material points at the entire layers using equation (3). The value of the undrained shear strength are shown in Figure 13 at the ground surface and in Figure 14 for the quick clay layer at top surface of the quick clay layer. The undrained shear strength is correlated with the elevation such that the deeper the soil layer, the higher the undrained shear strength. That is consistent with the CPTUs data in which the undrained shear strength increases linearly with depth in the normally consolidated clay. The source code, data, and instructions for reproducing the numerical results presented in this paper can be found on the open-source platform GitHub.

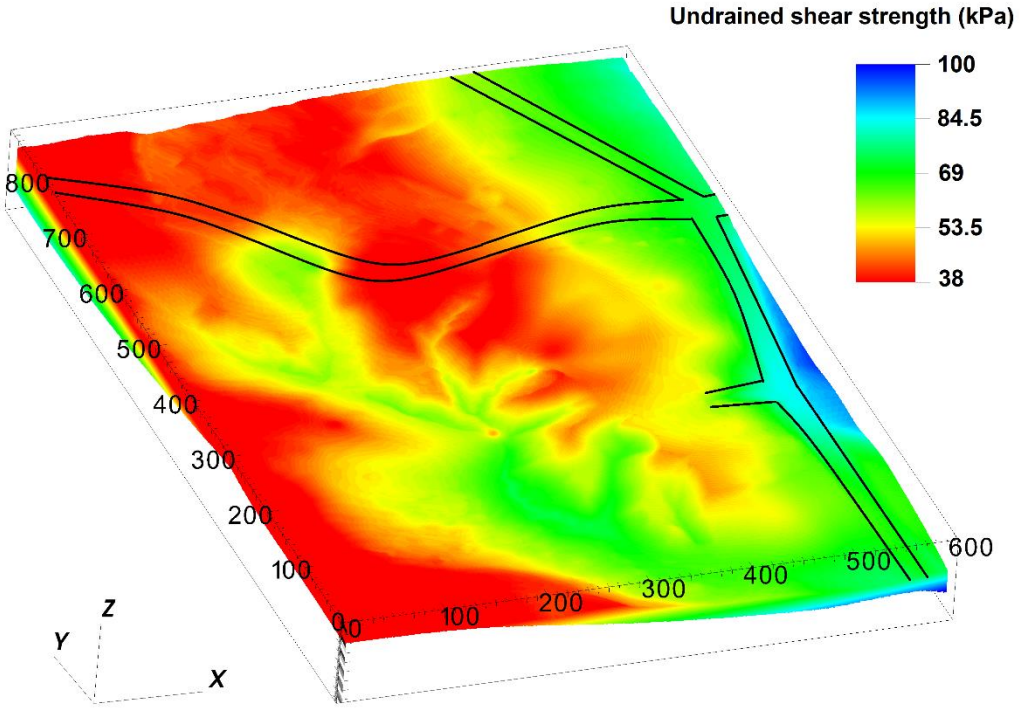

192

193 **Figure 13 The undrained shear strength at the ground surface**

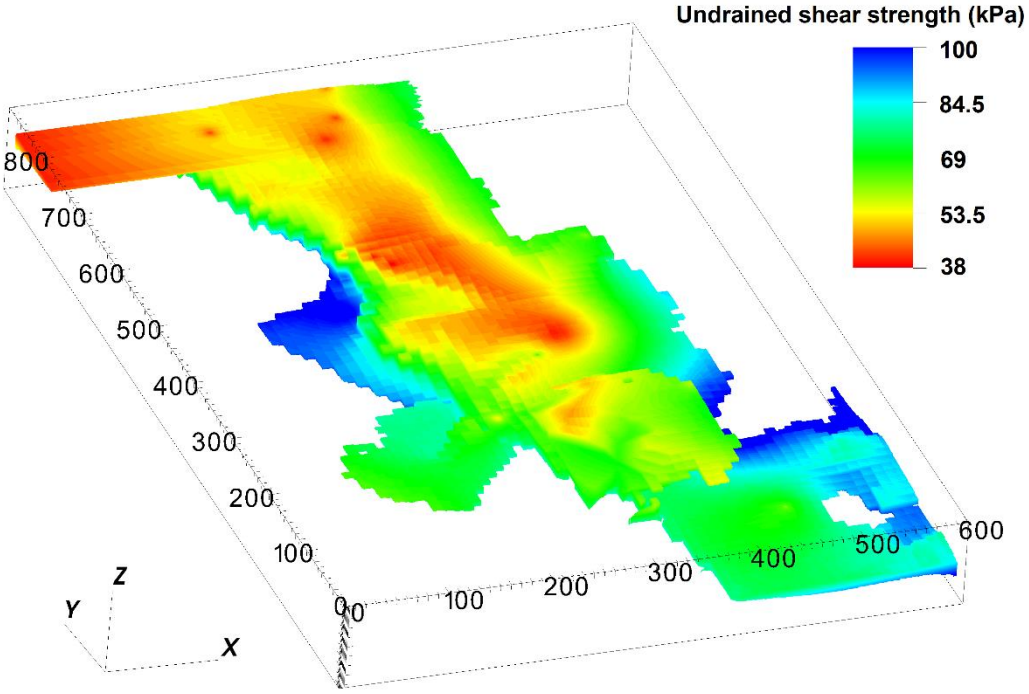

194

195 **Figure 14 The undrained shear strength on top of the quick clay layer**

5 Numerical model

5.1 Generalized Interpolation Material Point Method

The Material Point Method is a continuum method well suited for the solution of dynamic large deformation problems. Comparing the Material Point Method to the Finite Element Method where the integration points are fixed in the deformed mesh, the Material Point Method allows the integration points, or more precisely the material points, to move freely in the background mesh (see Figure 15). As a result, large deformations in solid mechanics can be modeled for materials that are history dependent. Several years later, Bardenhagen and Kober (2004) proposed the Generalized Interpolation Material Point Method (GIMP), which significantly improves the robustness and accuracy of the original Material Point Method. The GIMP version of the Material Point Method is used in this paper.

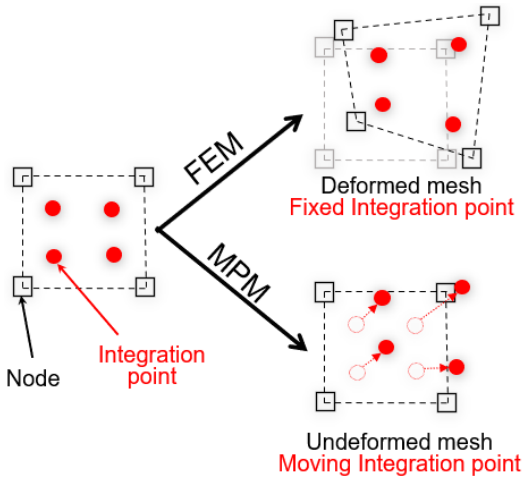

Figure 15 Material Point Method vs Finite Element Method (FEM)

5.2 Geotechnical parameters

Table 1. Parameters in the progressive failure of the quick clays slope

Layer	$s_{u,ref}$ (kPa)	s_{ur} (kPa)	$S_t = \frac{s_{u,ref}}{s_{ur}}$	γ_{95}
non-sensitive clay	CPTUs data	10	1-10	25%
quick clay	CPTUs data	0.5	20-100	25%

Based on the soil investigation (Multiconsult, 2021a), the average soil unit weight is 19.5 kN/m^3 for all layers. For undrained condition, the Young's modulus is set to be 10 MPa with the Poisson's ratio of 0.49. Sensitivity analysis showed that elastic parameters have negligible effects on the numerical results.

According to NS8015 (Toril Wiig, 2020), quick clay has a remolded undrained shear strength of less than 0.5 kPa. Therefore, the quick clay layers were calculated using remoulded undrained shear strengths of 0.5 kPa. Meanwhile, CPTUs data indicated that the minimum undrained shear strength in some boreholes is 11 kPa. Therefore, we select a remoulded undrained shear strength of 10 kPa for the non-sensitive clay layer. The sensitivity of the clay layer is between 1-10 and the sensitivity of the quick clay layer is between 20-100, which corresponds to the results of the fall cone tests in the Gjerdrum landslide (Multiconsult, 2021a). Due to the mesh dependence of this parameter, the parameter γ_{95} (accumulated shear strains required to obtain 95% reduction of shear strength) governing the softening rate is scaled in accordance with the mesh. In several studies (Rogstad, 2021; Tran & Solowski, 2019), γ_{95} was set to be approximately 100% for mesh sizes of 0.25 m. Using the scaling law, it corresponds to γ_{95} of approximately 25% for a mesh size of 1 m. The constitutive soil parameters for the study are summarized in Table 1.

6 Numerical results

6.1 Phase 1: pre-failure initial stress condition

Phase 1 of the simulation is dedicated to establishing the initial stress conditions. All layers are placed within the rigid bedrock, while all side boundaries operate under Neumann boundary conditions, which facilitates the free movement of debris out of the domain in Phase 2. Phase 1 involves the generation of initial stresses through gravity loading, utilizing estimated topography data from 2007 and incorporating the undrained shear strength of the soil. A density value of 1950 kg/m^3 for saturated clay is considered during this process to establish the initial

236 total stress condition. To expedite equilibrium attainment, numerical damping is applied,
237 ensuring efficient progression to the steady state in the simulation. It is important to note that
238 the numerical damping introduced in Phase 1 is later removed during the second phase of the
239 simulation, allowing for a more precise representation of the system's behavior during the
240 retrogressive failure analysis in Phase 2. To initiate the calculation in Phase 2, the topographical
241 differences between 2015 and 2007 were removed to mimic erosion. This unloading process
242 acted as a trigger for the initiation of retrogressive slides.

243 **6.2 Phase 2: initiation of the first slides**

244 The Gjerdrum landslide was initiated by first local instability near Tistilbekken. It is likely that
245 one or more small slides were triggered down the eastern slope of Tistilbekken during the early
246 morning of 30th December 2020. As we transitioned from Phase 1 to Phase 2 and removed the
247 soil mass near the slope's toe, it became evident that these slopes initially exhibited very low
248 stability, with a safety factor of approximately 1. Due to the instability and the low strength
249 and softening behavior of quick clays, the numerical model showed that first slides occurred
250 without additional numerical intervention. Here are some numerical observations during the
251 initiation of the slide:

252 - The numerical model indicated the location of the first slides in a manner that reported
253 in the Gjerdrum report (Ryan et al., 2021) as illustrated in Figure 16 where the blue
254 color indicates the speed of the first soil blocks at about 10 seconds after the Phase 1.
255 At the location of the first slide, the quick clay layers are shallow just few meters below
256 the ground (at 166 m in Figure 11, compared to the terrain's elevation of around 170 m
257 in Figure 9).
258 - In addition to predicting the movement of the first slides, the numerical model showed
259 a 3D propagation of shear bands or a very thin weak layers along the toe slope near the
260 creek as illustrated in Figure 17 where the blue color indicates the magnitude of the

shear strain at the surface. These shear band were primarily governed by the morphology of the quick clay layers and initiated the retrogressive failure of this quick clay landslide.

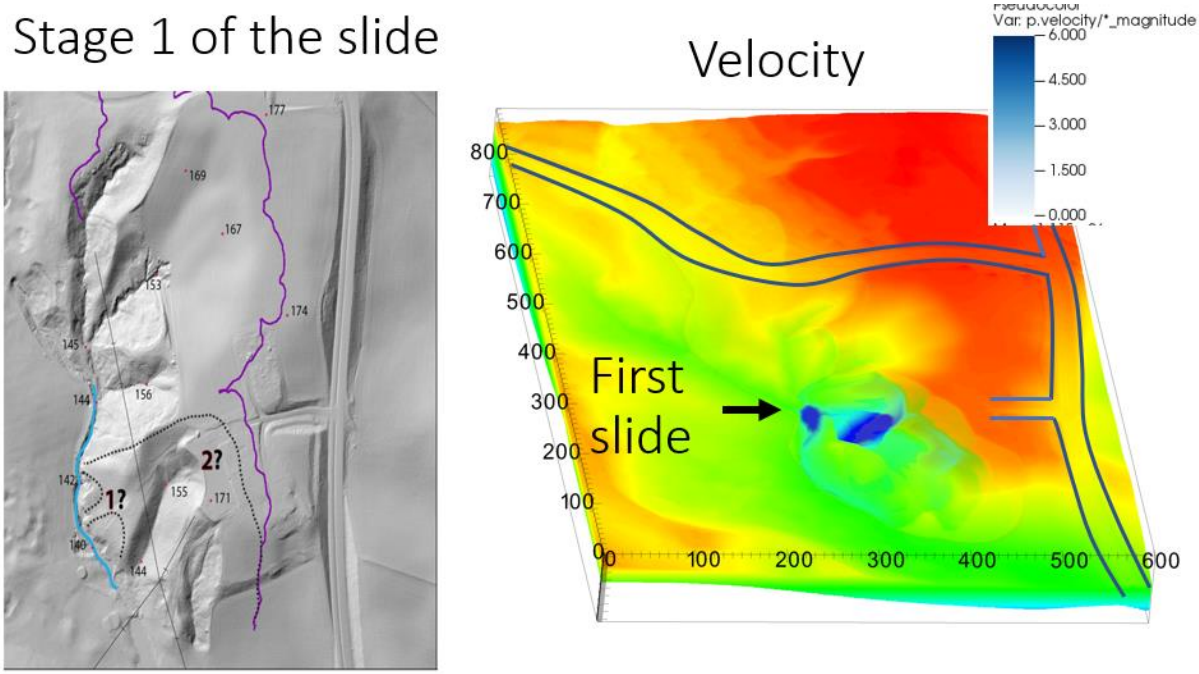

Figure 16 Numerical prediction of the location of the first slides, velocity in m/s

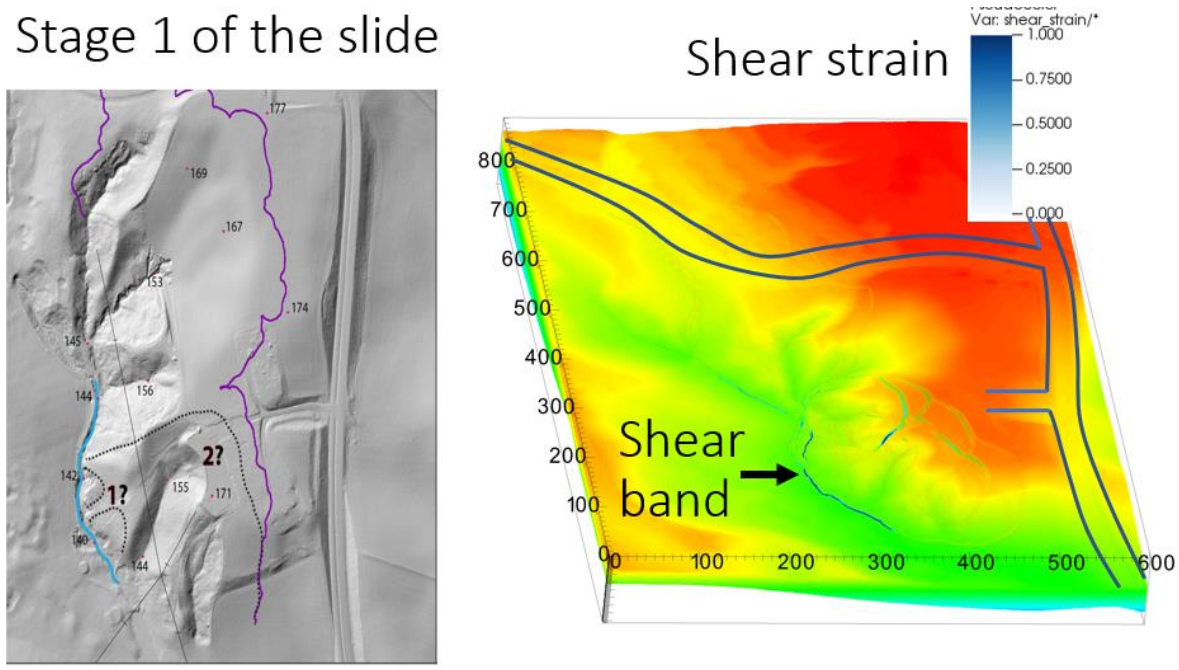

Figure 17 Development of shear band during the initiation of the first slides

6.3 Phase 2: retrogressive failure mechanism after the first slide

This section illustrates the retrogressive failure in the 3D numerical model and draws a comparison with the on-site observations. The initial slides in the Gjerdrum landslides were reported to trigger a pattern of backward-propagating fractures, following which the landslide masses flowed southwestward (stages 0, 1, 2 in Figure 3). The quick clay on the slope west of Holmen was stirred and flowed away, leaving a steep, unstable slope to the north. Consequently, retrogressive failure occurred with quick clay debris flowing mainly southward. In Stage 7, the landslide event hit Nystulia, and the landslide masses destroyed buildings along the western side of the landslide area.

Using the numerical model, the entire retrogressive failure can be captured as shown in Figure 18 for snapshots taken at 20 seconds, 50 seconds, 60 seconds, and 120 seconds, with the blue color indicating the magnitude of the shear strains. Approximately 20 seconds after the first slide, the soil remoulded and flowed southwestward (the black arrow in Figure 19 indicates the direction of the landslide mass movement in the numerical model). The shear bands/fractures propagated to the north at 50 seconds (see the black dashed line in Figure 19). Retrogressive failure occurred immediately following the propagation of the shear band at 60 seconds, with remoulded quick clay flowing mainly to the south. On the east side of the landslide, the soil mass collapsed after 60 seconds due to the remoulded clay continuing to liquefy. Further soil movement to the west was induced because of this. This soil movement was overestimated in comparison with what was observed on site. At 120 seconds in the simulation, the final deposition can be observed.

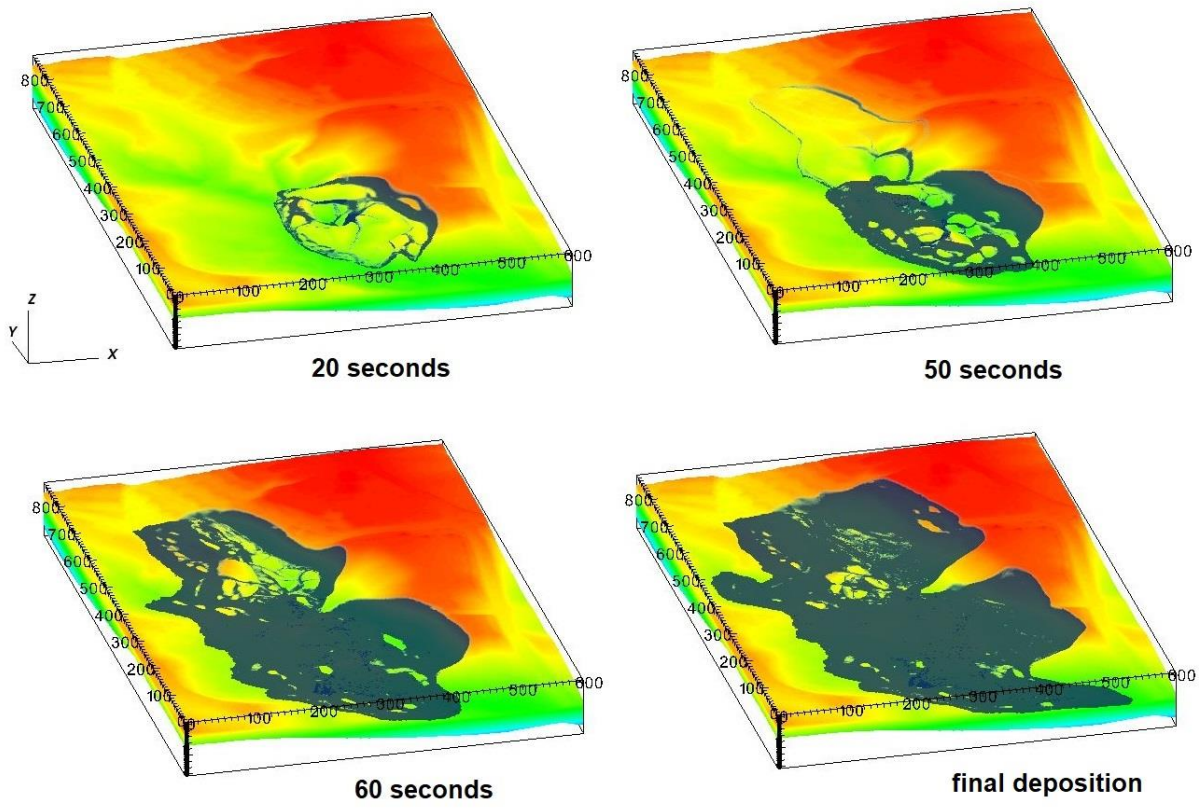

Figure 18 Progression of soil movement following initial slides, blue color indicates shear strain magnitude

In Figure 19, the position of two cross sections A-A and B-B are presented to provide more comprehensive understanding of the simulation process. They were selected to illustrate the main movements and the directions of the debris flow. The development of the shear zones with time are shown in cross-sections A-A and B-B in Figure 20 and Figure 21.

Cross-section A-A (Figure 20) shows how the first part of the landslide flows westward 20 seconds after initiation. According to the Varnes' classification of landslides (Hungr et al., 2014), the failure mechanism as seen in cross section A-A after 20 seconds is a **rotational clay slide**. This is due to the sliding of the soil mass along a rotational rupture surface. Rapid movement of the quick clay is involved. Notably, this initial slide does not consistently align with the quick clay layer in the numerical simulation. This is since the peak strength is rather similar in the sensitive and the non-sensitive clay. The difference in the behaviour of quick

clays compared to non-sensitive clays become apparent during the retrogressive continuation of the slide mechanism and is caused by the loss of strength in the quick clay (it liquefies).

The cross-section B-B (Figure 21) clearly display this **retrogressive flow development.** Failure is characterized by a rapid flow of liquefied sensitive clays with multiple retrogressive clay blocks dislocated and remoulded. Most of these slides closely align with the quick clay layers, except for the first and last slides. The slides propagate along the quick clay layer and cease when there is no longer quick clay present.

In summary, the simulation effectively depicts the progression of the Gjerdrum landslide. The simulation overestimate soil mass movement, approximately 50 meters westward, by the end of the retrogressive process (Figure 19). Figure 20 illustrates the quick clay layer in green and again it may be seen that the first shear band did not consistently follow this specific quick clay layer. This divergence is because the failure initiates at low shear strains, where the quick clay still retains a significant amount of shear strength before shear strength degradation occurs.

The retrogressive development, as depicted in Figure 21, demonstrates a strong alignment between shear band retrogressive development and the quick clay layers, with the retrogressive failure ending when the failure mechanism reach the end of a quick clay layer.

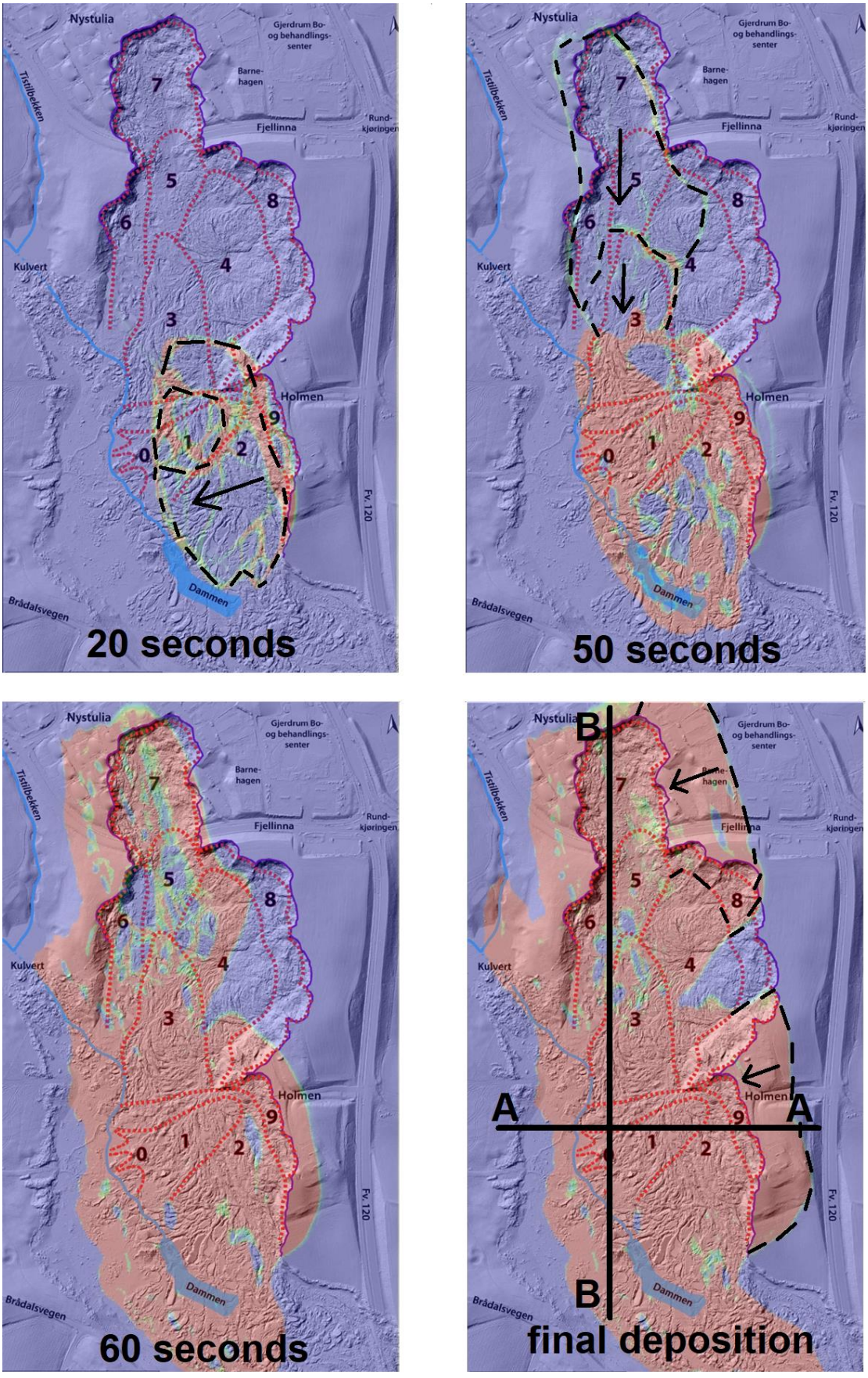

Figure 19 Development of shear band following initial slides, red color indicates Displacement Magnitudes

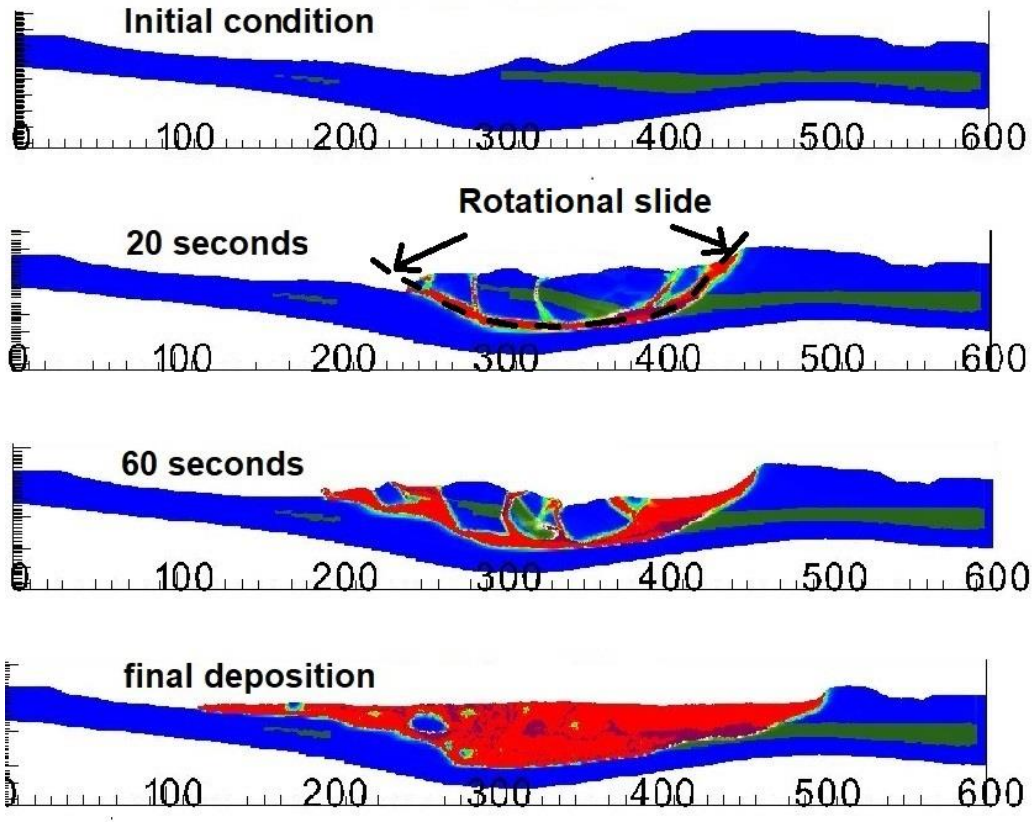

Figure 20 Development of shear bands along cross section A-A, green indicates intact quick clay layer, red indicates shear strain magnitude.

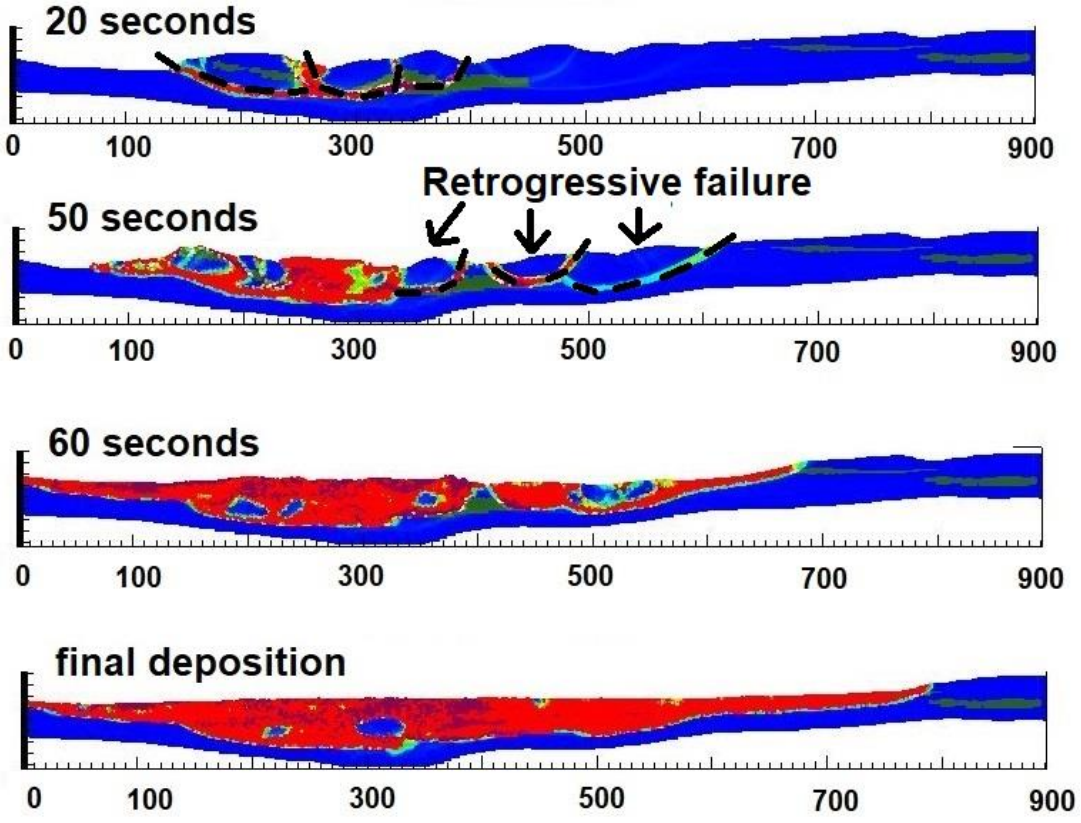

Figure 21 Development of shear bands along cross section B-B, green indicates intact quick clay layer, red indicates shear strain magnitude.

6.4 Influence of softening rate in retrogression distances

In this section, we examine the influence of softening rate on the failure mechanism of sensitive clay landslides. The undrained shear strength is governed by equation (1). Thus, softening behavior is in our model governed by two parameters. The first parameter is the remoulded undrained shear strength of the clay s_{ur}. The second parameter is the accumulated shear strain required to obtain a 95% reduction in shear strength γ_{95}. The former reflects the sensitivity of clay S_t, while the latter controls how quickly a material will soften. A sensitivity analysis was performed to investigate the effects of softening on the development of the retrogression distance (how far back the slide mechanism will go). With limited softening (a less sensitive clay) the regression would have been moderate, and the slide would not reach the houses in Nystulia. Such a case is simulated and shown in Figure 23. Unfortunately we had a highly sensitive, quick clay in Gjerdrum, and the simulation with the corresponding "high sensitivity" parameters are shown in Figure 24 The slide reached the houses with tragic consequences. The simulations illustrate the importance of modelling the loss of strength (softening) correctly.

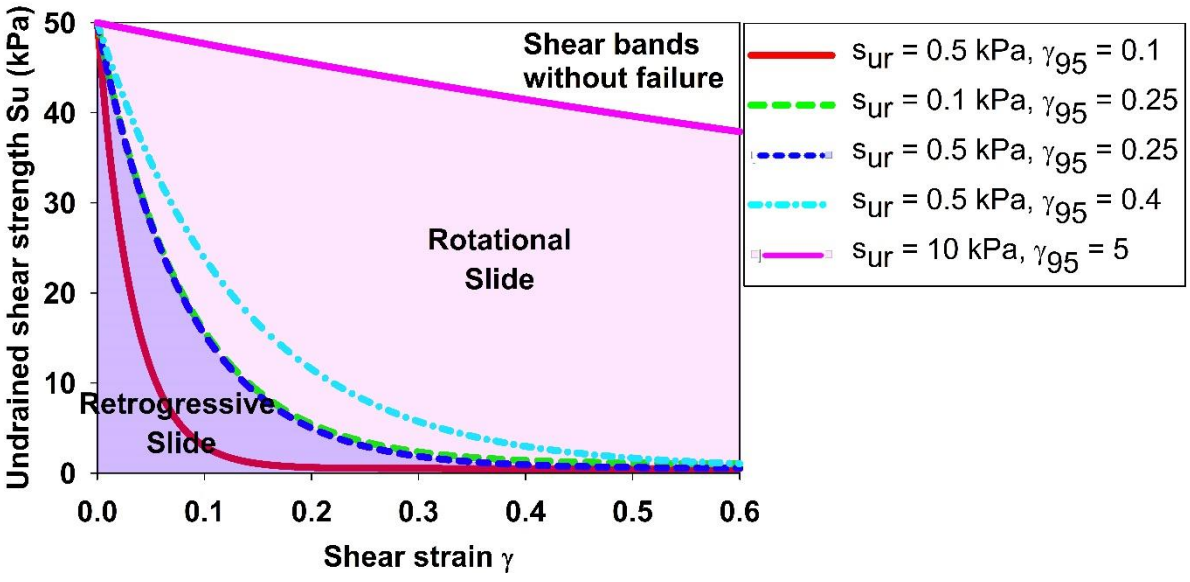

Figure 22 Influence of stress-strain curve in the failure mechanism

The sensitivity analysis suggested that there are three different mechanisms as illustrated in Figure 22 that depend on the softening rate of the material. In Figure 22 a peak shear strength

of 50 kPa is assumed reduced to values shown on the vertical axis as a function of accumulated shear strain. Several sets of softening parameters are used.

(1) For no or limited softening we may see no failure: This is the case for the upper right corner in the diagram. No failure occurs for remoulded undrained shear strength larger than 10 kPa and γ_{95} equal to or less than 5.

(2) Rotational slides: If the clay has a high sensitivity and a high softening rate, the slope fails but shows primarily rotational slides with limited retrogression as illustrated in Figure 20. Therefore, the retrogressive distance was moderate. If this was the clay in Gjerdrum the houses would not have been reached according to our simulation. Unfortunately, the Romerike quick clay is more sensitive than this.

(3) Retrogressive slides: When the clay has an extremely high sensitivity and significant rate of softening, such as in Gjerdrum, typically remoulded undrained shear strength of 0.5 kPa and γ_{95} less than 0.25, then our simulation show a retrogressive slide as in Figure 21. For the clay with just slightly less softening rate such as γ_{95} of 0.26, the slope fails with primary the rotational slide. As a result, the retrogressive distance was higher and closer to what was observed on site as shown in Figure 24 (houses reached). Reducing either the remoulded undrained shear strength and/or γ_{95} from the threshold s_{re}= 0.5 kPa; γ_{95} = 0.25 had negligible effects on the final retrogressive distances because the landslides almost reached the vicinity of the bedrock layer.

Our study demonstrates the influence of softening rate on the failure mechanism of the quick clay landslides.

However, this analysis is based on the hypotheses that (a) each layer of soil is homogeneous, and the undrained shear strength were calculated from equation (1) that was used to average the mechanical behavior of the clay; (b) the softening law was constructed

with the mesh size of 1 m with scaling law to prevent the strain localization. This scaling method has been shown to mitigate mesh dependence in landslide analysis (Tran & Solowski, 2019). Therefore, numerical analysis using other mesh sizes require scaling adjustment.

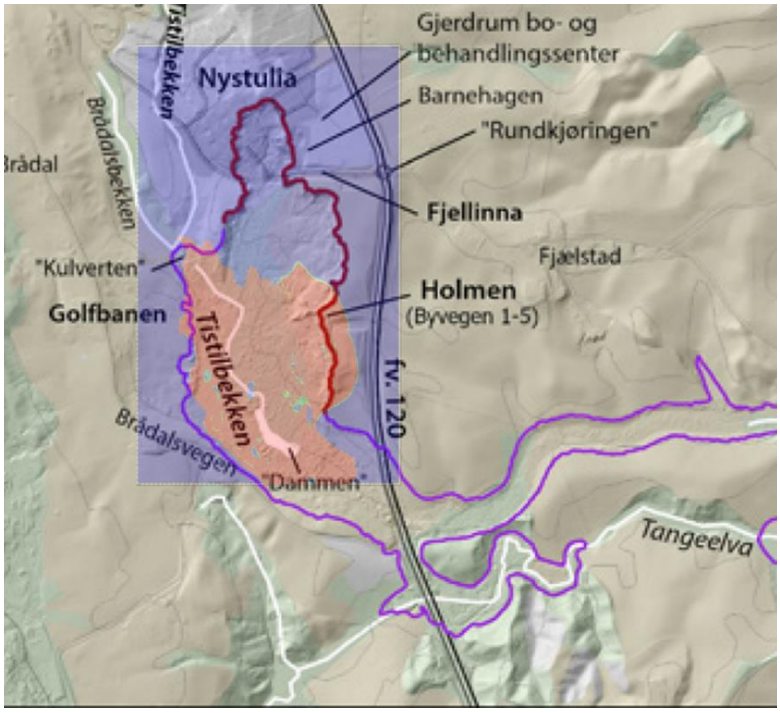

Figure 23 Prediction of retrogression distance in the case of rotational slides

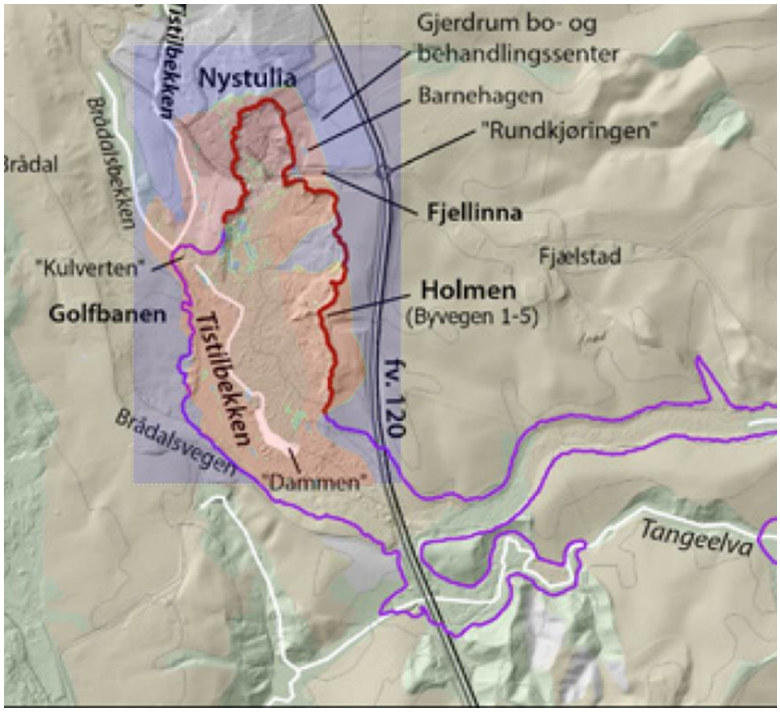

Figure 24 Prediction of retrogression distance in the case of retrogressive slides

7 Conclusion

In the existing literature, numerical analyses of sensitive clay landslides are often conducted using 2D models. Nevertheless, there are evidence that 2D and 3D models can yield notably distinct outcomes. Consequently, we have developed a 3D model specifically tailored for analyzing the retrogressive failure of the quick clays. This study rigorously compares our model with real-world observations from the Gjerdrum landslides, revealing a high degree of alignment between our numerical predictions and on-site observations.

One distinctive aspect of our model is its ability to integrate three critical elements: (1) the reconstruction of a 3D terrain coupled with intricate layers of quick clays; (2) the assignment of 3D soil properties based on Cone Penetration Test (CPTU) data; and (3) the computation of retrogressive distances and the onset of failure within a unified framework, employing large deformation analysis utilizing in the Material Point Method. Our model provides a tool to explore the progressive/retrogressive nature of quick clay slides in three dimensions. In addition to serving as an alternative to empirical methods, it offers the capability to predict retrogressive distances as well as run out distances for debris material. However, further studies are needed to give possible recommendations for parameters and findings, enabling utilization of this method in evaluation of possible impact areas in hazard mapping.

Moreover, our research quantifies the impact of the softening rate on sensitive clay layers, which is a critical factor governing the failure mechanisms of sensitive clay landslides. Notably, our numerical findings suggest that the initial shear band may not be strictly confined to propagating exclusively along the quick clay layers. Instead, it's plausible that shear bands align with the quick clay layers during the retrogressive process. This is as expected.

It's essential to acknowledge certain limitations of our model: (1) The 3D numerical model is presently limited to total stress analysis; (2) Accurate detection of sensitive clay layers and precise characterization of soil properties are prerequisites for good simulations.; (3) The

computational demands are substantial, necessitating access to high-performance computing facilities.

To achieve a more comprehensive understanding of failure mechanisms of sensitive clay landslides, the pursuit of effective stress analysis should be considered for future research.

8 Acknowledgements

The authors gratefully acknowledge Dr. Samson Abate Degago from Norwegian Public Roads Administration for constructive discussion. The research received support from the European Union's Horizon 2020 research and innovation program under the grant agreement 101022007. The computations were performed on High Performance Computing resources provided by UNINETT Sigma2 - the National Infrastructure for High Performance Computing and Data Storage in Norway.

9 Code availability

Instructions for replicating the numerical results in this paper are given at the open-source platform GitHub. Also, the open-source code is shared in this platform for interested users to take up and make use of the results.

10 Reference

Alison McQuillan, N. B., T. Yacoub. (2021). On the comparison of 2D and 3D stability analyses of an anisotropic slope. RIC2021: Rocscience International Conference, Toronto, Canada.

Dey, R., Hawlader, B., Phillips, R., & Soga, K. (2015). Large deformation finite-element modelling of progressive failure leading to spread in sensitive clay slopes. *Geotechnique*, *65*(8), 657-668. https://doi.org/10.1680/geot.14.P.193

Fernandez, F., Vargas, E. D., & Velloso, R. Q. (2020). A 3D discretization procedure for the material point method (MPM). *Computational Particle Mechanics*, *7*(4), 725-733. https://doi.org/10.1007/s40571-019-00303-7

Grimstad, G., Nordal, S., Solberg, I.-L., & Ottesen, H. B. (2022). Om kvikkleire og skredet den 30. desember 2020 i Gjerdrum. *Naturen*, *146*(2-3).

Hungr, O., Leroueil, S., & Picarelli, L. (2014). The Varnes classification of landslide types, an update. *Landslides*, *11*(2), 167-194. https://doi.org/10.1007/s10346-013-0436-y

J.S. L'Heureux, O. A. H., A.P. Paniagua-Lopez, S. Lacasse. (2018). Impact of climate change and human activity on quick clay landslide occurrence in Norway. Second JTC1 Workshops on Triggering and Propagation of Rapid Flow-like Landslides, Hong Kong.

Liu, Z. Q., L'heureux, J. S., Glimsdal, S., & Lacasse, S. (2021). Modelling of mobility of Rissa landslide and following tsunami. *Computers and Geotechnics*, *140*. https://doi.org/ARTN 104388

10.1016/j.compgeo.2021.104388

Locat, A., Jostad, H. P., & Leroueil, S. (2013). Numerical modeling of progressive failure and its implications for spreads in sensitive clays. *Canadian Geotechnical Journal*, *50*(9), 961-978. https://doi.org/10.1139/cgj-2012-0390

Locat, A., Leroueil, S., Bernander, S., Demers, D., Jostad, H. P., & Ouehb, L. (2011). Progressive failures in eastern Canadian and Scandinavian sensitive clays. *Canadian Geotechnical Journal*, *48*(11), 1696-1712. https://doi.org/10.1139/T11-059

Multiconsult. (2021a-a). *0226192-01-RIG-BER-001 rev00 Teknisk beregningrapport – Parametere*. O. Multiconsult.

Multiconsult. (2021a-b). *10226192-01-RIG-BER-001 rev00 Teknisk beregningrapport. Parametere* (Oslo: Multiconsult, Issue.

Rippa, S. (1999). An algorithm for selecting a good value for the parameter c in radial basis function interpolation. *Advances in Computational Mathematics*, *11*(2-3), 193-210. https://doi.org/Doi 10.1023/A:1018975909870

Ryan, I., Ottesen, H. B., Nordal, S., Bruvoll, A., Hæreid, G. O., Solberg, I.,, & al., e. (2021). *Årsakene til kvikkleireskredet i Gjerdrum 2020*.

Toril Wiig, S.-A. S. o. E. D. H. (2020). *Sikkerhet mot kvikkleireskred*. N. v.-o. energidirektorat.

Tran, Q. A., & Solowski, W. (2019). Generalized Interpolation Material Point Method modelling of large deformation problems including strain-rate effects - Application to penetration and progressive failure problems. *Computers and Geotechnics*, *106*, 249-265. https://doi.org/10.1016/j.compgeo.2018.10.020

Virtanen, P., Gommers, R., Oliphant, T. E., Haberland, M., Reddy, T., Cournapeau, D., Burovski, E., Peterson, P., Weckesser, W., Bright, J., van der Walt, S. J., Brett, M., Wilson, J., Millman, K. J., Mayorov, N., Nelson, A. R. J., Jones, E., Kern, R., Larson, E., . . . Contributors, S. (2020). SciPy 1.0: fundamental algorithms for scientific computing in Python (vol 33, pg 219, 2020). *Nature Methods*, *17*(3), 352-352. https://doi.org/10.1038/s41592-020-0772-5

Zhang, X., Wang, L., Krabbenhoft, K., & Tinti, S. (2020). A case study and implication: particle finite element modelling of the 2010 Saint-Jude sensitive clay landslide. *Landslides*, *17*(5), 1117-1127. https://doi.org/10.1007/s10346-019-01330-4